REVIEW ARTICLE

Check for updates

Recent advances in layered double hydroxide (LDH)-based materials: fabrication, modification strategies, characterization, promising environmental catalytic applications, and prospective aspects

Amal A. Altalhi,[a] Eslam A. Mohamed 🆔 *[b] and Nabel A. Negm 🆔 *[b]

Layered double hydroxides (LDHs) are clay networks with brucite ($Mg(OH_2)$) layers that are coupled with anions between the produced layers. The building structure of LDHs follows the formula $[M_{1-x}^{2+}M_x^{3+}(OH)_2]^{x+}(A^{n-})_{x/n} \cdot yH_2O$, where M^{3+} and M^2 are trivalent and divalent cations in the structural units (sheets), respectively; x is the M^{3+} to ($M^{2+} + M^{3+}$) cation ratio of the structure; and A^n is an interlayer anion. LDHs can be created utilizing simple approaches that regulate the layer structure, chemical composition, and shape of the crystals generated by adapting production parameters. The first method of modifying LDH composites is through intercalation, involving the insertion of inorganic or organic precursors into their composition, which can then be employed for a variety of purposes. The next method is a simple physical mixing technique between the created LDHs and advanced materials, such as activated carbon, graphene and its derivatives, and carbon nanotubes, for utilization as base substances in energy storage, supercapacitors, photo- and electrocatalysts, water splitting, and toxic gas removal from the surrounding environment. The final strategy is the synthesis of polymer–LDH composites by inserting effective polymers during the manufacturing process of LDHs to create nanocomposites that can be utilized for energy, fire retardant, gas barrier, and wastewater cleaning applications. LDHs are a type of fine chemical that can be designed to have a desired chemical structure and performance for various purposes, such as redox reactions, bromination, ethoxylation, aldol condensation, NO_x and SO_x elimination, and biofuel production. Because LDH substances are not harmful to the environment, their different applications are unique in terms of green chemistry as they are recyclable and eco-friendly catalysts. The present review investigated the various methods used to create LDHs and the improvement of the produced composites *via* enhanced temperature calcination; intercalation of their structures by small-, medium-, and high-nuclear anions; and support by carbon compounds. The evaluation methods and the best prospective uses, such as biofuel generation, catalysis, water splitting, charge transfer, and wastewater treatment, are comprehensively reported according to the most current studies, and the future directions of LDHs are highlighted.

1. Introduction

Layered double hydroxides (LDHs) are made up of two metal cations, divalent and trivalent, in the form of double layers or lamellar structures. Anions (nitrates, sulfates, or carbonates) and water molecules essentially fill the interlayer gaps between the metal hydroxide layers.[1-3] The general formula for LDHs is

$[M_{1-x}^{2+}M_x^{3+}(OH)_2]^{x+}(A^{n-})_{x/n} \cdot yH_2O$, where M^{2+} and M^{3+} are the divalent and trivalent metal cations, respectively; A^{n-} is the related anion; and x is the ratio of $M^{3+}/(M^{2+} + M^{3+})$, where ($0.1 < x < 0.5$). Furthermore, the M^{2+}/M^{3+} ratio must be in the range of $1-6$[4-6] to produce LDHs. From an industrial standpoint, LDHs come from brucite, or mineral clay, which is mostly made of $Mg(OH)_2$. An equivalent amount of trivalent metal cations (M^{3+}) replaces a portion of divalent metal cations (M^{2+}) during the production of LDHs based on brucite. Consequently, positive charges are left on the surface of the layers, which are balanced by water molecules and comparable anions that occupy the interspace among the layers. The assembly of

[a] *Department of Chemistry, College of Science, Taif University, P.O. Box 11099, Taif 21944, Saudi Arabia*

[b] *Egyptian Petroleum Research Institute, Nasr City, Cairo, Egypt.*
*E-mail: eslamepri@gmail.com, nabelnegm@hotmail.com*
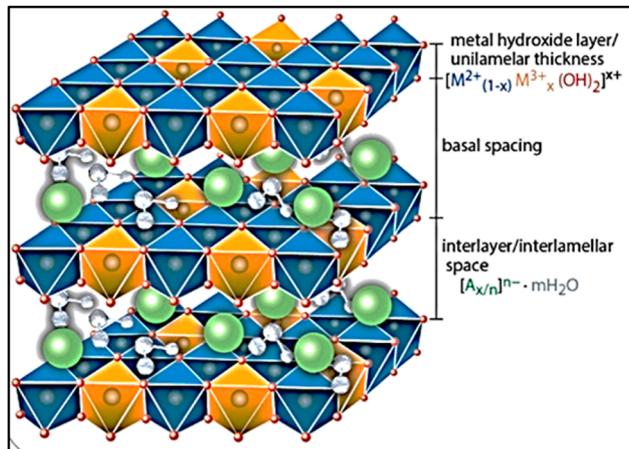
Fig. 1 Distinctive gaps and distances of the layered double hydroxides.

the lamellae and the formation of distinctive LDH structures are supported by the compensation of anions of the generated positive charges.[7] The hydroxide layers are contained in the cores of octahedral structures (Fig. 1), and the cations M^{2+} and M^{3+} are uniformly distributed throughout the lamellar structures.[6,8]

The LDH structures are stabilized due to the electrostatic interaction among the positive charge layers and the negative charge anions present amongst these layers. The density of the remaining positively charged layers and the number of negative charge anions connected to the construction can be established by the ratio among the M^{2+} and M^{3+} cations in the framework of the LDH layers. The valence of the cations and the relationship between the different ion types significantly affect the layered double hydroxide characteristics, particularly their porosity, ion exchange propensity, and crystallinity.[9]

2. Techniques applied for LDH preparation

Different techniques are used to create layered double hydroxides. Every technique may provide a distinctive product with certain characteristics mostly in terms of surface area, shape, crystallinity, and physical and chemical characteristics. The co-precipitation technique, hydrothermal approach, and sol–gel technique are the most often used techniques for creating layered double hydroxides.

2.1 Method of co-precipitation

The most popular technique for creating double hydroxides is co-precipitation. This involves vigorously spinning diluted solutions of metal cation salts at certain temperatures between 50 and 90 °C.[10–12] Then, by employing NaOH or NH_4OH in the existence of a perfectly appropriate concentration of carbonate salt in the form of Na_2CO_3, the medium's pH is changed to alkaline, precipitating the produced metal oxides. The reaction time and the alkalinity of the medium have the ultimate impact on the creation of the layered double hydroxides. At a pH of 9–12, for 24 hours under stirring conditions and drop-wise titration, the shape, surface area, and crystallinity of the resulting layered double hydroxides improve.[13] However, this methodology results in the combination of counter hydroxide ions in/on the inter-outer layers of LDH.[14] The co-precipitation method offers numerous advantages, including a high yield, one-step synthesis, crystalline LDHs, and high purity.[15]

2.2 Hydrothermal approach

The layered double hydroxides are prepared using the hydrothermal technique at temperatures as high as 180 °C and under pressure. Production environments, such as the temperature and time of the hydrothermal process, play a vital role in defining the crystallinity of the prepared LDHs. The hydrothermal technique is predominantly appropriate when foreign organo-anions with low affinity need to be assimilated into the prepared LDH interlayers. The hydrothermal technique has several advantages, such as controlled particle dimensions, morphology, and the presence of only hydroxide anions in crystal lattices.[16] This procedure may be used for the initial reactants or after the metal cation mixing.[17] Sharp crystals and a large surface area are characterized by the layered double hydroxides that are produced when hydrothermal procedures are used at higher temperatures.

2.3 Sol–gel technique

The sol–gel approach includes the occasional employment of acetates and acetyl acetonates as anions. The anion salts are disseminated in an organic solvent, and the hydrolysis of the alkoxides is performed to obtain a sol matrix. Then, mixing the medium creates the required LDHS, which results from the colloidal phase gel that forms due to internal cross-linking. The characteristics of the resulting LDH are frequently improved by amending the condensation rate, pH, temperature, and solvent-type metallic precursors during hydrolysis. The produced LDHs *via* the sol–gel approach had high purity, a large surface area, and precise pore-size.[18,19]

In comparison between the different routes, the most famous routes used for preparing LDHs are co-precipitation, hydrothermal, and sol–gel. Several advantages and disadvantages have been reported for the obtained products using these methods. The co-precipitation route involves simple stages and equipment with economical, rapid, and scalable LDH yields. However, the obtained LDHs lack effective control over the crystallinity and lattice arrangement. The hydrothermal route is used for large-scale production of LDHs with effective controlling of the crystallinity and morphology, with a longer reaction time and higher energy. The sol–gel route permits the preparation of either nanostructure characterized by high crystallinity and regular morphology after a long reaction time, while powder LDHs have low crystallinity at a short reaction time.[20]

3. Calcination of layer double hydroxides

Layered double hydroxides undergo lamellar structural reorganization at high temperatures due to the calcination process.
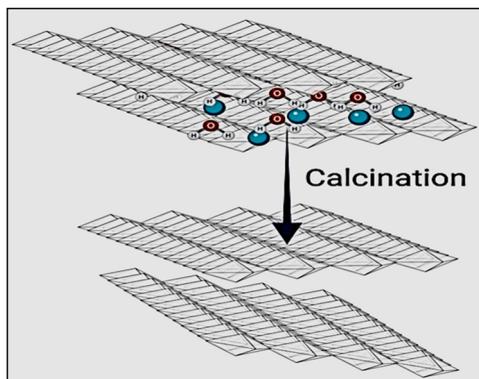
Fig. 2 Mixed metal oxides in a 3-D LDH network.

Fig. 3 X-ray diffraction patterns of NiMo/LDH.

Fig. 4 SEM of NiMo/LDH.

Mixed metal oxides are created as a result of this process, which enhances the formation of the octahedral to the tetrahedral crystalline structure of LDH. More positively charged cations are formed due to this process as a result of the defects formed in the crystalline structures. The creation of defects in the produced crystalline structures serves as compensation for these charges. These defects include the presence of oxygen in the structure and cationic vacancies.[21–24] To produce the matching 3-D framework of diverse metal oxides (Fig. 2),[25] three kinds of reactions took place through the calcination of LDHs: the first reaction is the dehydration of adsorbed and interlayer water molecules, then dehydroxylation of the layers, followed by the decomposition of the anions.

4. Physicochemical methods of LDH characterization

Several methods are often used to study layered double hydroxides, including Fourier transform infrared spectroscopy (FTIR), X-ray photoelectron spectroscopy (XPS), scanning electron microscopy (SEM), X-ray diffraction (XRD), and thermogravimetric analysis (TGA).

4.1 XRD spectroscopy

The most important spectroscopic technique for determining the created LDH degree of crystallinity, the arrangement of the generated layers, and the gaps between them is their XRD diffraction profile. Each LDH has a unique fingerprint that reveals its crystalline and geometrical arrangement, which may be interpreted as a sign of the structure's acceptable quality and purity. JCPDS file no. 22–700 identifies the distinctive sharp, thin, and symmetric reflections relevant to the low values of 2-theta (θ) of typical basal planes (003), (006), and (009) of the hydrotalcite structure.[26] Moreover, it demonstrated the emergence of wide and asymmetric reflections at the 2-theta of the non-basal (012), (015), and (018) planes (Fig. 3). Regardless of the production process, the characteristic 2-theta values of the various LDHs remain constant, while the variation is found in the d-spacing between the LDH layers, which is determined by the size and kind of intercalated ions that exist among the layers.
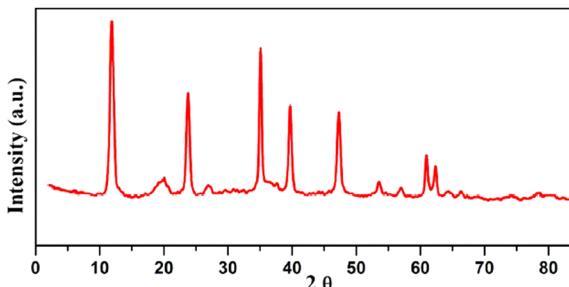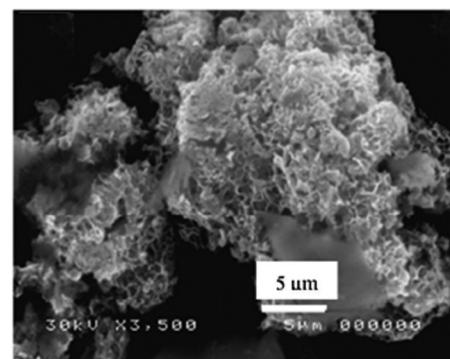
4.2 SEM analysis

Scanning electron microscopy (SEM) is useful for imaging the hydrotalcite structural unit of the LDH framework (Fig. 4). Highly porous plate-like crystalline arrangements in a hexagonal-ordered crystal structure are often observed in the SEM pictures of layered double hydroxides.[26]

4.3 FTIR analysis

The distinctive bands of the hydrotalcite compounds are depicted in the FTIR chart of the LDH. The stretching of hydroxyl groups and the insertion of H_2O molecules between the layers of LDHs were attributed to the wide and broadband at 3400 cm^{-1} (Fig. 5). For example, concerning the Zn/Al–CO$_3$ LDH, the interlayer bridging of H_2O–CO_3^{2-} is the cause of the
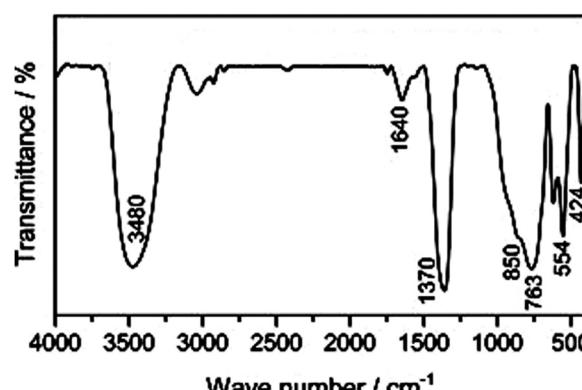

Fig. 5 FTIR spectra of ZnMgAl-LDHs (Zn/Mg = 0.125).

shoulder at 3050 cm^{-1}. The H$_2$O bending deformation is represented by the band at 1630 cm^{-1}. The asymmetric stretching of CO$_3^{2-}$ groups is identified by the strong bands at about 1370–1380 cm^{-1}. For the Al–O groups, Zn/Al–OH translation, and Al–OH deformation, the bands at 460, 550, and 790 cm^{-1} may be supported, respectively.[27]

4.4 X-ray photoelectron spectroscopy (XPS)

One important technique for determining the chemical composition, evaluating the oxidation states, and analyzing the electronic structure of layered double hydroxide surfaces is XPS[28] (Fig. 6).

4.5 DTA-TGA

DTA-TGA investigations examine weight changes under the influence of temperature. TGA calculates the mass variation of the compounds under various gas or atmospheric conditions, both during heating and cooling. One well-known form of LDH is the TGA of the Zn–Al LDH, which shows that when the temperature rises, it also determines the loss of interlayer or adsorbed water content as well as the intercalated CO^{3-}, NO^{3-} groups, and SO$_4^{2-}$. According to the thermogravimetric investigation of Zn–Al LDH by Wang and co-authors (Fig. 7), the loss of interlayer water content at the 50–250 °C range resulted in a loss of weight of around 10–14%.[29] The thermogram for Zn–Al–CO$_3$ revealed two phases at 150 °C and 250 °C, accompanied by a 21% loss. The dehydration of adsorbed and interlayer water caused the first inflection (at 150 °C), while the loss of CO^{3-} groups within the LDH interlayers caused the second inflection. Four thermogram phases have emerged for Zn–Al–NO$_3$ LDH at 150, 250, 350, and 450 °C. The loss of interlayer and surface water molecules caused the first two

Fig. 7 Typical thermogram profile of Zn–Al LDH (blue line: DTA scaled on the right vertical axis; black line: TGA scaled on the left vertical axis).

steps. The dehydroxylation of Zn–Al LDH and the breakdown of the interlayer nitrate anions were responsible for the second two phases, which occurred at 350 °C and 460 °C and resulted in an overall loss of 21.5%.

Advanced methods have been reported for the characterization of different LDHs. Raman analysis is considered a diagnostic tool for LDHs, and it is widely employed to identify the presence of foreign anions in the interlayer among brucite-like sheets. Consequently, this technique is always used in combination with others.[30] Yang et al. studied the adsorption mechanisms of Cr(VI) by LDH intercalated with EDTA through a multi-approaches analysis, which involved XRD, FTIR, X-ray photoelectron spectroscopy (XPS), and zeta potential analysis.[31]

The Raman spectrum of the LDH sample (Fig. 8) showed the presence of Fe^{2+} and Fe^{3+} ions in its structure. A sharp band at 1506 cm^{-1} strongly indicated the presence of Fe^{3+} ions,[32] and

Fig. 6 (a) Fe 2p, (b) Mg 1s, (c) O 1s, and (d) C 1s orbital XPS spectra for the FeMg/LDH.
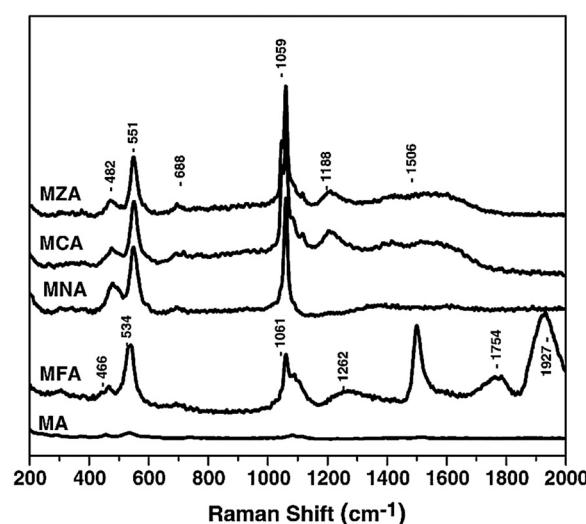
Fig. 8 Raman spectra of the different LDH samples.

the band at about 1927 cm^{-1} corresponded to species of Fe^{2+},[33] which suggested the co-existence of both Fe^{2+} and Fe^{3+} species in the sample. The presence of Fe^{2+} ions was due to the reduction of Fe^{3+} to Fe^{2+} during intercalations. The partial reduction of Fe^{3+} to Fe^{2+} might be associated with the hydrogen bonding between the interlayer water molecules or hydroxyl groups of the LDH sheets and the Fe^{3+} cations. As assigned above, the bands at 1061 cm^{-1} and 1262 cm^{-1} were assigned to the vibrations of the carbonate species $(CO_3)^{2-}$.[34]

A commonly employed way to characterize nanosized materials is to couple transmission electron microscopy (TEM) and selected area electron diffraction (SAED) analysis. Hobbs *et al.*[35] applied *in situ* TEM to comprehensively characterize LDH nanomaterials. The combined approach of TEM and SAED allowed for both a morphological and crystallographic understanding of the LDHs (Fig. 9).

A novel approach for the characterization of LDHs was reported by Dionigi *et al.*,[36] which combined operando X-ray scattering and absorption spectroscopies to elucidate the active phase and the mechanism for the oxygen evolution reaction (OER) application. Despite previous reports on the *ex situ* crystal structure of the as-synthesized precursors of M/Fe LDH catalysts and the *in situ* local structure based on XAS measurements, little was previously known about the long-range crystal structures of the catalytically active phase during application conditions. Combining electrochemical measurements and operando wide-angle X-ray scattering (WAXS), XAS data with computational simulations that were specifically for the strongly correlated Fe, Co, and Ni oxides and (oxy)hydroxides assisted in unraveling the crystal structures and electrocatalytic OER mechanisms of the active phases of Ni/Fe and Co/Fe LDH catalysts.

5. Promising LDH uses

The unique nanostructure of layered double hydroxides, the occupancy of multiple metal cation types within their layers, the active –OH groups on their surface, the simplified preparation routes, the non-toxicity, the flexible changing of both cations and anions, the outstanding anion replacement ability, memory retention, the highly efficient transport of the intercalated anion in a sustained mode, the bio-compatibility, the electrochemical activity, the high surface and pore size, the high adsorption capacity and efficacy make LDH composites a promising category of the nanomaterials. LDH and its intercalated form with various functional precursors, as well as nanocomposites containing superior nanomaterials, primarily carbon nanomaterials, are regarded as effective precursors for essential applications because of their remarkable properties. Applications for LDHs and their modified forms include water splitting, wastewater treatment, oil transesterification for the manufacture of biofuel, and catalysis.

5.1 Biofuel manufacture using the transesterification process catalyzed by LDH

Transesterification and pyrolysis are the two primary procedures used to produce biofuels from oils and fats.[37,38] Triglycerides and short-chain alcohols combine during the transesterification process to produce a fatty acid (FA) monoester.[39–41] Pyrolysis is the process of heating triglycerides without the use of catalysts (thermal cracking) or with catalysts (catalytic cracking).[42–46]

Because of the presence of metal oxides and the electropositivity of the cations present in their composition, LDH acquired active sites that are effective during the transesterification reaction and can be classified as Lewis-base catalysts.[47] The chemical
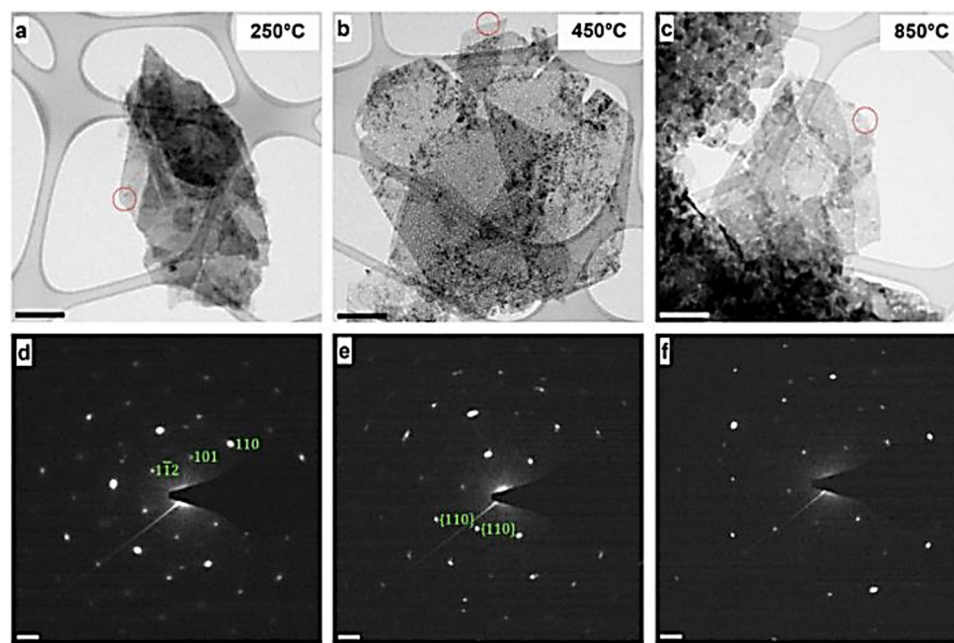
Fig. 9 Transmission electron microscopy (TEM) images (a–c) and associated selected area electron diffraction (SAED) patterns of the Ni/Fe LDH (d–f).

activity of the layered double hydroxides was enhanced by the various metal cations present in their structures. It makes sense that the temperature at which the cations are calcined, as well as their valence and ionization states, affect the catalytic activity.[48] Numerous reports have discussed the function of the basic sites of mixed oxides and the other physical–chemical characteristics of the transesterification process.

Using the co-precipitation approach, LDH with the formula $[Mg_{(1-x)}Al_x(OH)_2]^{x+}(CO_3)_{x/n}^{2-}$ (x = 0.25–0.55) was created.[49] To create the appropriate biodiesel, the obtained materials were added through the transesterification of glyceryl tributyrate in the presence of methyl alcohol. As the magnesium concentration increased, the conversion rate increased. The comparative research conducted by Boey et al. between thermally treated crab shells and laboratory-prepared CaO revealed no discernible differences in the CaO sources used in the transesterification reaction of palm oil to biodiesel.[50] Li–Al, Mg–Al, and Mg–Fe were the three produced calcined LDHs that were employed to create the appropriate biodiesels by methanol utilizing two triglycerides: glyceryl tributyrate and soybean oil.[47] In terms of fatty acid methyl ester yields, Li–Al layered double hydroxide showed the maximum activity when used at 65 °C, but Mg–Fe and Mg–Al LDH showed lower activity. In contrast to the large concentration of weak basic sites on the surfaces of Mg–Al and Mg–Fe LDH, the greater activity of Li–Al LDH was ascribed to the existence of a high concentration of the medium and strong basic sites on its surface. These results were obtained using CO_2-TPD spectroscopy, offering a clear picture of the different kinds and intensities of active sites on the catalyst surface. The greatest activity for Li–Al was attributed to the noncrystalline nature of lithium aluminate due to the structure breakdown into the equivalent mixed oxide at the calcination temperature of 450–500 °C. Similar findings were reported by Sankaranarayanan et al.,[51] who found that calcined Ca–Al$_2$ LDH exhibited great activity in converting non-edible and edible oils into biodiesels. The high basic characteristics of the catalyst, which were ascertained using Hammett CO_2-TPD elucidation, were credited with the activity of the used Ca–Al$_2$ LDH.

The adsorption of the reactants occurs on positions of the catalyst surfaces known as the active sites, as part of the transesterification reaction process that has been described in many phases.[52,53] In the transesterification media, the LDH acts as a heterogeneous catalyst and is supplied as solids alongside glycerol and biodiesel. One significant benefit of heterogeneous catalysts is their ease of separation and recycling.[54]

A categorical and motivating transesterification mechanism was proposed and reported.[55] During this mechanism (Scheme 1), the initialization step is initialized due to the basic nature of the LDH catalysts. In the reaction mechanism cycles, cycle 1 presented the abstraction of the protons in the hydroxyl group of the alcohol (methyl alcohol) as the influence of the basic sites of the LDH to obtain the methoxide anions. In cycle 2, the formed methoxide anions attack the carbon formed by the carbonyl groups found in the oil molecules to form an intermediate (alkoxycarbonyl), easily degenerating into fatty acid methyl ester (FAME) and diglyceride molecules. In the final stage, the diglyceride anions containing the

oxygen attacked the proton linked to the LDH base, leading to the formation of the catalytic sites. Subsequently, a series of interactions occurred for the di-glycerides and the mono-glycerides to form the final product of the biodiesel molecules.

The mechanism of catalytic transesterification of waste cooking oil (WCO) using ZnAl/LDH@SiO$_2$ was reported by Fereidooni et al.,[56] as illustrated in Fig. 10. As reported, Si atoms are prone to connect to oxygen atoms in triglyceride, which highly supports electrophilicity on sites of triglyceride carbonyl. Consequently, the loading of SiO_2 on LDH sheets promotes the oxygen atoms to interact, accelerates the attack of the triglyceride carbonyl group by the methoxide molecules and increases the catalytic activity of LDH.

5.1.1 Structural factors affecting LDH activity in the biofuel manufacturing process. The preparation conditions and methods for layered double hydroxides have a significant impact on the surface characteristics of the hydroxides. The LDH calcination process, the medium's acidity or basicity, the reaction temperature, the concentration of the reacted metal ions, and the reaction duration are all considered preparatory conditions. Co-precipitation, hydrothermal, sol–gel, and other methods are among the preparation techniques.[57]

5.1.1.a LDH calcination procedure. The components of layered double hydroxides are reorganized significantly during the heat treatment (calcination process).[23] The catalytic activities of layered double hydroxides, such as the activity of the basic strength reactive sites and the increased reactive surface area, are supported by this procedure.

5.1.1.b Basicity of LDHs and basic locations. The occurrence of deformation in the catalyst's crystalline structure explains the creation of the basic site mechanism. Metal oxides are incorporated into the distorted crystals as a result of calcination, offsetting the positive charges that are produced. The fundamental active sites in the distorted system are produced by the presence of O^{2-} anion. When the created basic sites are found in the function groups OH^-, Mg–O, and O^{2-}, they may be categorized as weak, medium, and strong sites.[3]

5.1.1.c Metal ion doping in LDHs. It has been observed that the chemical structures of various metals may modify the surface basicity of layered double hydroxides, thereby changing their activity. Fe^{3+}, Cu^{2+}, and Zr^{2+} are the most reactivating metal ions. The layered double hydroxides doped by Cr^{3+}, Fe^{3+}, Cu^{2+}, Mn^{2+}, Co^{2+}, Ni^{2+}, and Zn^{2+} improved their catalytic activity throughout the transesterification process according to the CO_2-TDP analysis.[58]

5.2 Catalysis performance

The adaptable structure and adjustable basic characteristics of the layered double hydroxides explain their catalytic function and match their intended use.[59] As heterogonous base catalysts, LDHs have great selectivity and potential for a wide range of catalytic processes, mostly organic transformations (Scheme 2), such as condensation, redox reactions, alkylation, hydroxylation, isomerization, hydro-formylation, and transesterification.
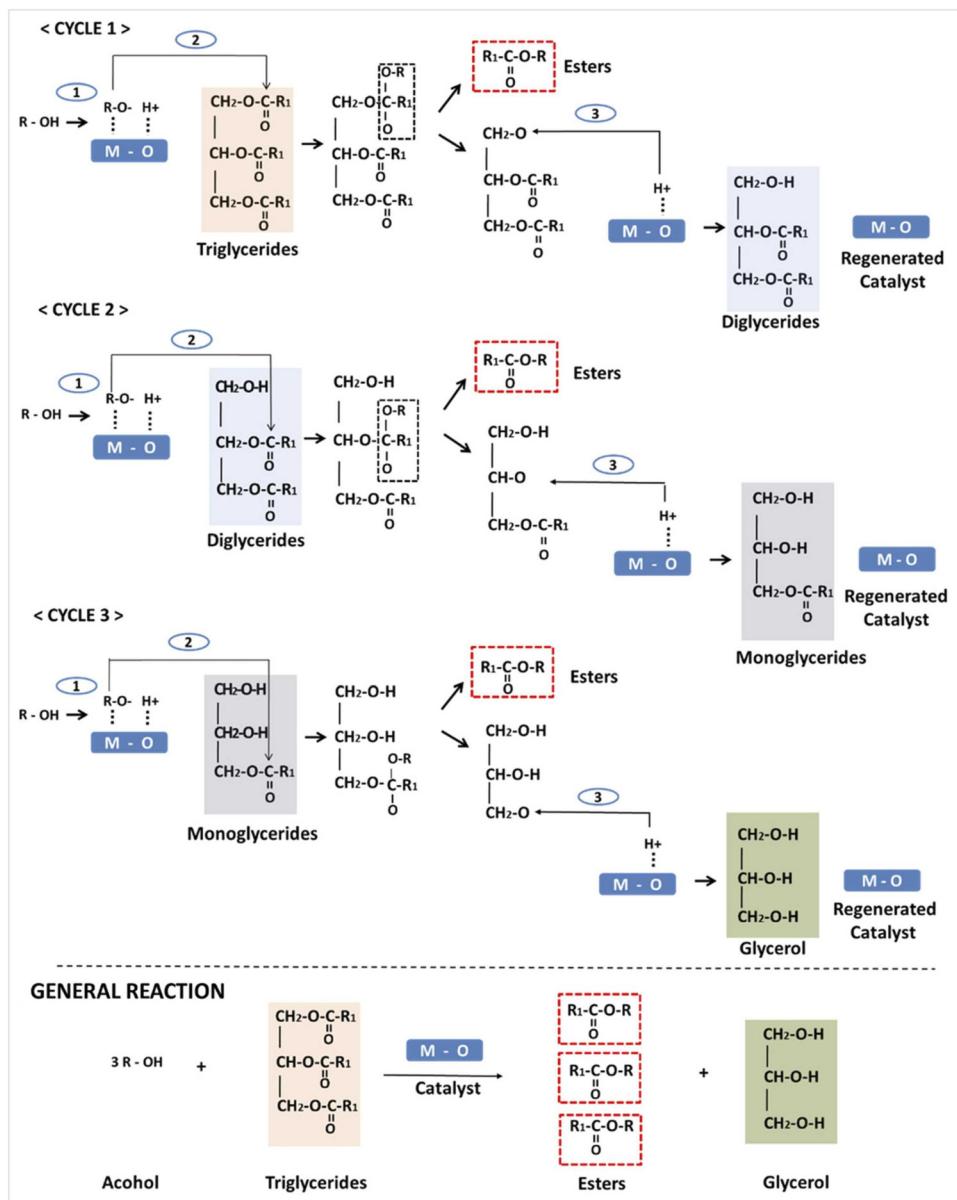
Scheme 1 Mechanism of transesterification.

Additionally, the mixed oxides resulting from the thermal treatment (calcination) of the LDHs show various organic reactions and worthwhile catalytic activity.[60]

Yan *et al.*[61–63] presented a concise review representing detailed information about the different mechanisms that occurred during the application of LDH composites in oxygen evolution reaction, hydrogen evolution reaction, urea oxidation reaction, nitrogen reduction reaction, and biomass derivative oxidation.

Lignin is one of the main constituents of lignocellulosic biomass and can provide an abundant source of aromatic compounds. The efficient utilization of lignin is believed to be a promising strategy for addressing the current energy crisis. However, the complex structure and rich oxygen-containing groups of lignin hinder its valorization into value-added

chemicals.[64] Hydrodeoxygenation (HDO) of biomass-derived derivatives has been widely considered an efficient and feasible strategy for removing excess oxygen content in lignin. LDHs are promising as suitable precursors for constructing bifunctional catalysts with both small-sized metal centers and acid sites for conversion reactions. Kai *et al.*[65] reported the conversion of vanillin (as a simulant for biomass comparable to lignin).

Both thermally modified and unmodified LDHs have found extensive application as stable, recyclable heterogeneous catalysts or catalyst supports for a range of processes, benefitting from the easy exchangeability of intercalated anions and the flexible tuneability and uniform distribution of metal cations in the LDH layers. Because of the availability of the hydroxyl groups, LDHs are attractive heterogeneous solid base catalysts for various chemical reactions. LDHs are converted to mixed
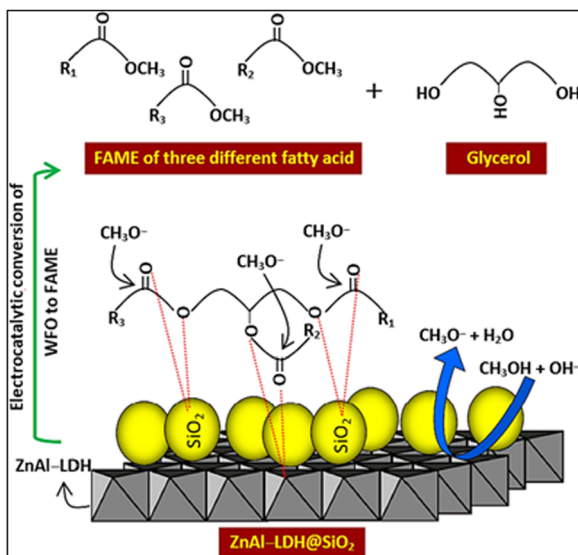
Fig. 10 Suggested mechanism of the transesterification process using the ZnAl/LDH-SiO$_2$ composite.

Scheme 2 Schematic of organic reactions catalyzed by LDH.
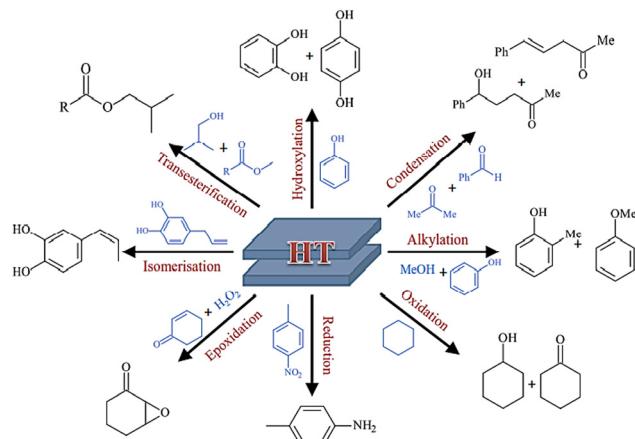
metal oxides with multiple Lewis base sites and increased surface area during heating between 450 and 500 °C, yielding good catalytic efficiency. In the absence of CO$_2$, the mixed metal oxide may be rehydrated to form LDH with an OH-intercalated anion.

5.2.1 LDH intercalation. The addition of a third cation to the binary LDH composites to create modified forms has an upsurging influence on their catalytic efficiencies while catalyzing the organic reactions. The type of cations used in the makeup of the intercalated anion determines the catalytic activity of the layered double hydroxides. Based on the size and chemical makeup of these anions, or nuclearity, the intercalated anions vary from one to another.

5.2.1.a Intercalated LDH with small nuclear polyoxometalate anions. Low-nuclear polyoxometalates (POM) are present in LDH systems and are primarily intercalated by chromate,
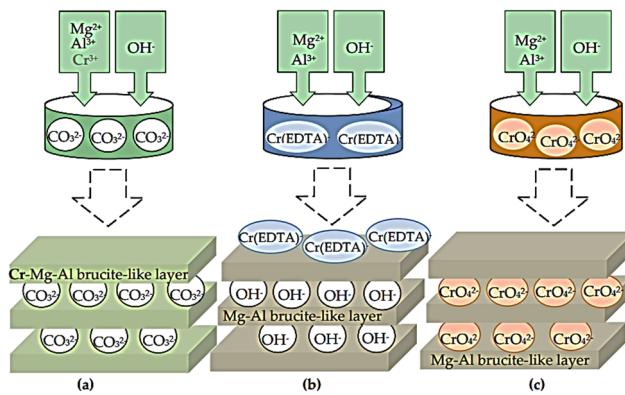
Scheme 3 Synthetic methods for producing chromium catalyst LDH precursors.

dichromate, and chromium anions, such as Cr-(EDTA) and [Cr-(SO$_3$-salen)]$^{2-}$. These LDH variants exhibited good catalytic activity, particularly in alcohol oxidation and alkoxylation. The intercalation of chromates in LDH is worthy of high consideration due to its applications in the remediation of wastewater and its valuable applications in the catalysis of numerous reactions with important products. CrO$_4^{2-}$ and Cr$_2$O$_7^{2-}$ anions are deceptive anionic contaminants found in wastewater.[66]

Co-precipitation, anion exchange, and reconstruction of the mixed oxide procedures have been reported as effective methods for the synthesis of LDH containing M^{2+}/M^{3+} cations interpolated with chromate in the brucite-like layers.[67–70] Scheme 3 shows the synthetic strategies used to prepare the LDH precursors of the chromium catalysts. These strategies include (i) co-precipitation of metal cations with carbonate counter-ion under basic conditions; (ii) co-precipitation of Mg(II) and Al(III) with EDTA chelate of Cr(III) to form a chelate of 1 : 1 stoichiometry with (EDTA), as EDTA is thermodynamically stable compared to Mg(II) or Al(III);[71] and (iii) co-precipitation of Mg(II) and Al(III) with CrO$_4^{2-}$ anions existing at the slightly excess concentration required for stoichiometry in the medium. Good catalytic activity was shown by the LDH-intercalated sulphonate–salen–chromium(III) during the selective oxidation of glycerin in the presence of 3% H$_2$O$_2$ to create dihydroxyacetone. This was explained by the sulphonate–salen–chromium(III) and the weak base LDH with a balancing effect on each other. A series of POM/LDH nanocomposites were made by Malherbe *et al.* using Cr^{2+} and Cu^{2+} cations to create layered double hydroxides, with CrO$_4^{2-}$ or Cr$_2$O$_7^{2-}$ anions intercalated among the LDH layers. The compounds have been evaluated in the catalytic synthesis of glycol ethers in the catalyzed ethoxylation process of butyl alcohol with ethylene oxide.[72]

The intercalated LDH with various chromium-based anions, such as chromate, dichromate, Cr-(EDTA)$^-$, and [Cr-(SO$_3$-salen)]$^{2-}$, are excellent catalysts for various catalytic reactions due to their low-cost of precursors, easy synthesis, and superior stability.

5.2.1.b LDH intercalated with medium-nuclear polyoxometalate anions. LDH composites intercalated with medium-nuclear

polyoxometalates may accept anions based on vanadium or molybdenum. Layered double hydroxides of molybdate and vanadate (Mo-LDH, V-LDH) have effective catalytic activity in oxidation and epoxidation processes.

5.2.1.b.1 Vanadates. The most documented methods for creating layered double hydroxides intercalated with vanadate anions include co-precipitation, anion exchange, reformation, and hydrothermal methods, which provide hosting of the vanadate anions between the M^{2+}/M^{3+} cations in the brucite-like layers. Depending on the building cations and the acidity or basicity of the solution, vanadium anions may be interlayered in the layered double hydroxides and can also be added as cation V(III) in the LDH of the brucite-type layers.

After pre-swelling with terephthalate, Villa *et al.* described a straightforward method for preparing decavanadate-intercalated LDH containing Mg^{2+} and Al^{3+} cations. This was achieved by the direct ion exchange of the nitrate precursor with a mildly acidic $NaVO_3$ medium. It was shown by the Raman, IR, and XRD patterns that there are decavanadate ($[V_{10}O_{28}]^{6-}$) anions in the interlayer area. Decavanadate-intercalated LDH synthesized is classified as an allylic and homo-allylic alcohol-specific epoxidation catalyst.[73] Maciuca *et al.* produced LDHs intercalated with decavanadate and pervanadate anions immediately in a procedure identical to this one. Through the catalytic oxidation process of tetrahydrothiophene to sulfolane in the presence of hydrogen peroxide, the oxidative catalytic activity of the produced LDHs was evaluated.[74]

5.2.1.b.2 Molybdate. The predominant molybdate anions are $[MoO_4]^{2-}$, $[HMoO_4]^-$, $[Mo_6O_{19}]^{2-}$, $[Mo_7O_{24}]^{6-}$, $[HMo_7O_{24}]^{5-}$ $[H_2Mo_7O_{24}]^{4-}$, and $[Mo_8O_{26}]^{2-}$. The intercalation of molybdenum-based anions in the structure of layered double hydroxides depends on the pH of the medium and the concentration of Mo(VI) cations. Due to the formation of heptamolybdate $[Mo_7O_{24}]^{6-}$ ions, which may be stable at low pH levels and increase the spacing between the brucite-type sheets, the intercalation of molybdates is inhibited in the interlayer space of layered double hydroxides.[75] Within the context of the MgAl-LDH composite, the anionic exchange approach is generally applicable during molybdate assimilation. A novel approach based on the traditional ionic exchange method was published by Soled *et al.*, and it involves the synthesis of an anion-pillared organic precursor, which is then substituted in acidic environments by an appropriate polyoxometalate anion.[76]

5.2.1.c Intercalated LDH with high-nuclear polyoxometalate anions. The majority of LDH systems containing high-nuclear polyoxometalates are intercalated by tungsten anions. The catalytic activity of layer double hydroxide intercalated with tungsten anions was shown to be effective in the oxidation of organosulfur compounds, such as benzo- and dibenzothiophene, as well as in the epoxidation of alcohols. Polyoxotungstates are present in many forms and sizes, possess set dimensions, and have a wide range of applications.[77] The temperature, the length of time it takes for LDH and polyoxometalates to react, and the medium's pH have a significant impact on how the intercalated LDHs are prepared inside tungstate-based anions.[78] The interlayers of the layered double hydroxides are intercalated by polyoxotungstate structures and have various forms, including Keggin, Dawson, and Finke types.

Methoxybromination of aliphatic olefins produces moderate chemoselectivity, but methoxybromination of aromatic and aliphatic olefins produces strong regioselectivity and stereoselectivity.[79] The use of Mg–Al–Cl-LDH and Ni–Al–Cl-LDH exchanged with tungstate in mild oxidative bromination reactions has been reported.[80] Organotungstic compounds with modified Mg–Al-hydrotalcite intercalated acted as catalysts for the epoxidation of cyclohexene. Anionic exchange and complexation with added phosphonic acid in the sheets were used to execute the modified Mg–Al-LDH.[81] Using nitrate LDH precursors as an initial material, polyoxometalates $[H_2W_{12}O_{40}]^{6-}$ and $[W_4Nb_2O_{19}]^{4-}$ were synthesized and intercalated in brucite-like layers of Mg–Al- and Zn–Al-LDHs by applying the anion exchange technique. Using hydrogen peroxide, the cyclooctene epoxidation process was catalyzed by the modified LDHs.[82] The LDH composite of Mg–Al–SiW$_{12}$O$_{40}$, Mg–Al–PW$_{12}$O$_{40}$, and LDH virgin Mg–Al-LDH enhanced the photocatalytic degradation of malachite green (MG).[83]

5.2.2 Layered double hydroxides reinforced with materials derived from carbon. Assembling hollow flower-like LDH and N-, S-doped graphene acting as support for Pd-NPs gave hollow inner and mesoporous hierarchical flower composites. LDH/nanocarbon catalysts have been significantly considered owing to their significance in various reactions, such as Michael addition,[84] Knoevenagel reaction,[85] Ullman reaction,[86] Sonogashira reaction, Heck reaction, and chalcone synthesis.[87] By intercalating LDH with reduced graphene oxide (rGO),[88] and multi-wall carbon nanotubes (MWCNT),[89] sandwich-like structures were produced. One of the main characteristics of LDH/carbon composites is interfacial electron transfer,[90] which is aided by the high electronic mobility of the carbon components. Due to the interaction with the less conductive LDHs, this results in charge redistribution. Enhancing electron transport is possible using carbon dot-based LDH/nanocarbon.[91,92] During glucose electro-oxidation, the Ni–Al LDH/CNT nanocomposite displays electro-catalytic activity instead of the Ni–Al LDH electrode or the CNT electrode.[93] This was ascribed to the capacity of the carbon nanotubes (CNTs) to move extra electrons between Ni ions and electrodes, as well as to encourage reactant diffusion across the given porous complex framework.[94] The high strength and reusability of LDH/CNT catalysts were important characteristics that characterized the LDH intercalated by carbon nanotubes during application. It was constructed using LDHs and had a high mechanical strength of CNT in its purest form. Furthermore, the effective regeneration of the catalytic active sites and high stability against leaching are achieved by the strong metal–CNT contact.

5.3 Water splitting

Hydrogen, as a sustainable energy source, is an alternative to conventional petroleum fuels for mitigating soil contamination and the development of warming gasses.[95] The generation of hydrogen from the water splitting reaction of water using photocatalytic reactions is a promising source of energy due to its environmental and clean resource. The water splitting

reaction under the influence of irradiation can occur when the energy of the conduction band is more negative than the reduction potential of the hydrogen protons to hydrogen atoms and the valence band is more positive than the potential of oxidation of oxygen atoms to oxygen anions. The photocatalytic water splitting reaction occurs through three stages: the photo-catalyst absorbs photon energy higher than the bandgap energy of the water, which generates electron rich (electron)/electron deficiency (holes), followed by migration to the surface of the photocatalysts, and finally the occurrence of the reduction/oxidation reactions between the formed charges and the water molecules to generate the hydrogen and the oxygen.[96]

For the LDH composites, the formed surface charges after generation are transferred to the active sites within a finite short time ranging from nano- to microseconds.[97] The initial two steps depend on the structure and electronic configurations of the LDH photo-catalysts. The high crystalline LHD has a positive influence on photocatalytic activity, and the density of the morphological defects acting as recombination centers between the generated carriers decreases as the crystallinity increases. The specific photocatalytic water splitting mechanism in the case of LDH composites occurs due to the excitation of electrons from the ground state into the excited state, followed by the separation of the formed charges as a result of the formation of positive holes and negative centers due to the excitation process, and the excitation occurs throughout d–d electronic transitions, metal-to-metal and ligand-to-metal charge transfer.[98]

The photocatalytic mechanism of Bi_2O_3/ZnO/$ZnMe_2O_4$ LDH was extensively reported in a study by Boumeriame *et al.*[99] Bi_2O_3NPs LDH shows the typical water splitting mechanism (O_2 generated in the VB of both moieties and the Ag particles being reduced on the CB) (Scheme 4). After the calcination, the photogenerated holes of Bi_2O_3 decrease the overall recombination rate by balancing the electrons from the CB of the ZnO and $ZnMe_2O_4$ matrices. In the case of $ZnAl_2O_4$, the band structure does not allow for water oxidation; thus, Bi_2O_3/ZnO/$ZnCr_2O_4$ presents a higher OER rate.

5.4 Formation defect

The deformation of LDH composites is performed mainly by doping foreign metal cations into their crystalline structures.

Doping with foreign metal cations to form single-phase ternary metal compounds could boost the HER and OER catalytic performance, such as Fe-doped CoP, Fe-doped Ni_2P, Co-doped Ni_2P, Co-doped FeS_2, V-doped NiFe LDH, and some other metal-doping in metal compounds.[100] Based on theoretical mechanism theories, introducing foreign cations can change the initial electronic structures according to two different metal 3d-orbitals and can also improve the absorption of Gibbs free energy toward intermediates, which improves the electro-catalytic activities.

The presence of electronic vacancies in d-metal-based compounds, such as oxygen, sulfur, and selenium, can modify their electronic configuration and enhance their electrocatalytic activities.[101] In the case of metal oxide catalysts, generating oxygen vacancies enhances the catalytic activity because the electrons tend to collect near the valence band maximum of metal oxides with oxygen vacancies to form electron rich centers. The electron-rich centers acted as catalytic active sites that stabilized the reactants and reaction intermediates. This lowers the activation energy barrier and consequently catalyzes electrochemical reactions.

5.5 Transfer of charges

Because modified layered double hydroxides (LDHs) have remarkable two-dimensional and compositionally variable structures, they have been investigated as catalysts for optical and electrochemical processes.[102] LDHs provide space and position separation of redox-reaction sites for the efficient production of hydrogen and oxygen through the water-splitting process. Because of their large adsorption capability and tunable band gap, they are suitable for the ionic exchange process (cation–anion exchange).[103] Additionally, the lamellar structures of LDH allowed for various cation and anion types as well as crystalline sizes, forms, and morphologies. These characteristics have a significant impact on the efficiency of charge transfer and separation, which in turn raises concerns about the photocatalytic energy process's efficiency.[104] The most recent changes to LDH have been made to its size, shape, electrical characteristics, and chemical structure. By selecting novel carbon supports, such as carbon quantum dots,[105] graphene oxide,[106] graphdiyne,[107] and graphitic carbon nitrides,[108] the electrical
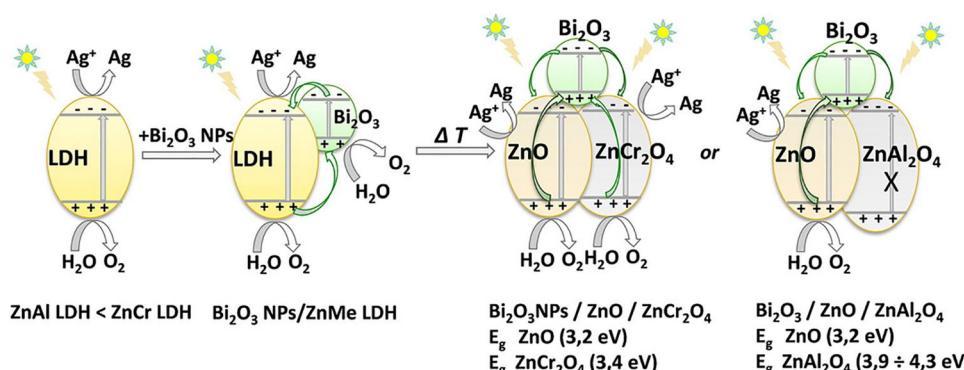
Scheme 4 Proposed mechanism for O_2-generation under solar-light irradiation over Bi_2O_3NPs/ZnMe-LDH and Bi_2O_3/ZnO/$ZnMe_2O_4$.

characteristics and charge separation capabilities were altered. These substrates possess the capacity to support the photo- and electro-catalytic properties of the layered double hydroxides.

In electro-catalytic processes, LDH materials with transition metal cations, particularly Ni and Co, have been widely used. In LDH hosts, the intercalation of POMs and simple metal oxyanions may result in photo-catalytic activity. The distinct lamellar structure and abundant active sites of LDHs containing various transition metals (*e.g.*, Co, Ni, and Fe) make them excellent electro-catalysts. A method for transforming inexpensive Fe substrates into ultra-stable electrodes for the oxygen evolution reaction was enhanced by Yipu *et al.*[109] This method was achieved using aqueous solutions containing oxygen and Ni^{2+} at room temperature to corrode Fe substrates. Instead of producing rust, this method produced nano-sheets of Fe-containing LDH on iron. According to Yan *et al.*, there was a significant improvement in the electrodeposit-support of graphene layers encircled by NO_3^- ions. The generated cerium dioxide in the nano-crystalline and amorphous forms of $Ni(OH)_2$ for the electro-catalytic oxygen evolution process showed a reduced over-potential value of 177 mV at 10 mA cm^{-2} current, with good durability reaching 300 hours at 1000 mA cm^{-2}.[110] Direct electro-deposition of nickel foam produced amorphous mesoporous Ni/Fe nano-sheets, which were then used as O_2-electrodes for the O_2 evolution process during the water-splitting reaction.[111] To deliver 500 mA cm^{-2} and 1000 mA cm^{-2} current densities at 240 mV and 270 mV potentials, respectively, the electrode demonstrated good efficacy through the water splitting reaction in an aquatic medium with a 200 mV potential.[111]

LDHs improved by various transition metal ions, including Fe, Co, Ni, Zn, and Mn, have been extensively studied. A series of catalysts, including metal oxides,[112] metal hydroxides,[113] metal selenides,[114] metal sulfides,[115] metal carbides,[116] and metal phosphides,[117] were established for the oxygen evolution reaction in an alkaline aquatic environment. Yang *et al.*[118] created LDHs modified by cobalt and nickel and intercalated their structures with $CoNiSe_2$ to catalyze H_2O-chemisorption and produce reactive hydrogen-containing intermediates, which effectively split water. Consequently, a layered double hydroxide hybrid structure was created by electro-depositing amorphous NiFe hydroxides on the surface of NiFeP.[119] The resulting catalysts exhibit strong electrical interactions that may be used to increase the water-splitting process by lowering the adsorption energy of water. By combining metal phosphides with NiFe-layered double hydroxides, one may concurrently perform a bifunctional oxygen evolution process of H_2 and O_2, making up for the shortcomings in each catalyst.[120,121]

5.6 Treatment of wastewater

The rapid advancement of industrial and agricultural growth is to be blamed for the massive and varied releases of pollutants into water bodies.[122,123] As a result of these advancements, many contaminants, such as metals, dyes, oxygenated anions, and emerging organic compounds, contaminate rivers and undersea environments. Wastewater is treated utilizing LDHs in several ways (Fig. 11).
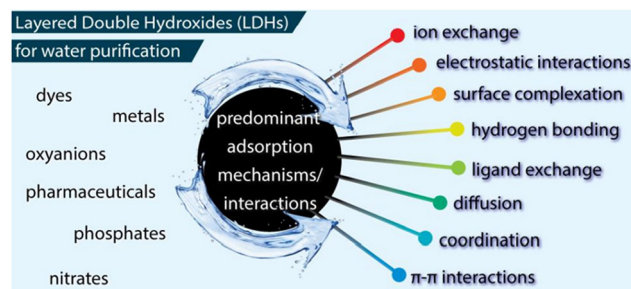
Fig. 11 LDH-based techniques used for wastewater cleaning.

Dyes are used in the food, pharmaceutical, paper, and textile industries. Approximately 10% to 15% of dyes are released into water resources by the textile industry. Because the dyes harm photosynthesis and, in turn, the concentration of oxygen in aquatic systems, their low concentrations pose harm to the environment. Moreover, hazardous and cancer-causing intermediates are produced by the degradation processes of many dyes.[124] Several industrial anionic and cationic dyes are effectively eliminated by LDHs.[125] When it comes to eliminating cationic and anionic dyes, respectively, LDHs and activated carbon behave in the same way.[126]

The excellent remediation effectiveness and adsorption capacity of several LDHs for the removal of cationic dyes have been widely documented.[125] Using the co-precipitation technique, two distinct layered double hydroxides (Mg–Al LDHs) were produced utilizing dodecyl sulfate (Mg–Al–DS) and carbonate (Mg–Al–CO_3), and their ability to uptake methyl orange from wastewater was evaluated. The maximum capacities for Mg–Al–DS and Mg–Al–CO_3 were 185.1 mg g^{-1} and 97.5 mg g^{-1}, respectively. The mechanisms of the adsorption reaction were proposed as the anion exchange of Mg–Al–CO_3 for methyl orange anion dye and the association of dye anions with the positive charges of LDHs.[127] The pH of the medium does not affect the efficiency of Mg–Al–DS LDH, but the efficiency of Mg–Al–CO_3 LDH is increased by an acidic to neutral medium.

The co-precipitation method was utilized to create carbonate anions LDH (Mg–Co–Al–CO_3 LDH), which was then used to remove RB19 dye from wastewater.[128] The produced LDH was proposed to play three roles: chemical bonding, physical adsorption, and electrostatic attraction. Using the precipitation approach, Ahmed *et al.* organized Mg–Fe-LDH nanoparticles and used them to adsorb Congo red dye from an aquatic medium. The physical and chemical interactions were the adsorption roles of the produced LDH.[125]

Large volumes of heavy metals, including cadmium, lead, mercury, copper, nickel, chromium, and arsenic, are discharged into the environment by industrial operations, particularly those related to batteries, electroplating, and mining. Transition metal ions are very poisonous and accumulate in nature.[129–131] The Satoshi Fujji group[132] was the first to describe using LDHs as adsorbents for Pb^{2+}, Cu^{2+}, and Zn^{2+}. The remediation of metal ions by layer double hydroxide has been described *via* several processes or interactions, including surface complexation, isomorphic substitution, surface precipitation, electrostatic interaction, and

chelation.[133] Ca–Fe double hydroxide LDHs were created by modifying them with 3-aminopropyl triethoxysilane. The nanocomposites were then assembled in 5% and 10% mixing ratios with polyaniline.[134] When Pb^{2+} ions were adsorbed from their aqueous solution, the produced composites were applied. The adsorption capacity of the LDH composite containing 10% polyaniline was 110 mg g^{-1}, while the one containing 5% polyaniline showed a capacity of 56 mg g^{-1}.

Using a microwave hydrothermal process, Zn–Ni–Cr double-layer hydroxides (Zn–Ni–Cr-LDHs) with a surface area of 354 m^2 g^{-1} were created and utilized to remove Cr^{6+} ions from the solution. With an optimal capacity of 28.2 mg g^{-1}, the produced adsorbent's suggested function was primarily an electrostatic contact between the Cr^{6+} ion and the adsorbent.[135] Three metal ions, namely Cd^{2+}, Pb^{2+}, and Cu^{2+}, were extracted from the aqueous solutions using Mg–Al-LDH intercalated with sodium alginate (SA-LDH).[133] For Cu^{2+}, Pb^{2+}, and Cd^{2+} metal ions, the produced LDH showed optimal capacities at 60 mg g^{-1}, 243.7 mg g^{-1}, and 95.6 mg g^{-1}. Precipitation, substitution, chelation, and bonding or complexation with hydroxyl or oxygen groups at the surface were the suggested functions of the produced LDH.

The lungs, kidneys, and heart are severely harmed by organic chemicals, particularly by benzene and poly-nuclear derivatives, including phenol, benzene, toluene, and xylenes. Although these pollutants are found in low quantities in water, their propensity to accumulate in all tissues makes their detrimental effects on the environment significant.[136]

The many types of anions present in wastewater, such as sulfates, nitrates, chromates, permanganates, arsenate, phosphates, selenates, and borates, are among the oxygenated anion pollutants. At low concentrations, these anions are dangerous to people.[137,138] Phosphate oxo-anions were adsorbed from their aqueous solution using zirconium-modified Mg–Al-LDH, which were made utilizing the co-precipitation process, followed by the calcination process to produce the oxide form Zr-LDH.[139] The maximal adsorption capabilities of Zr-LDH and Zr-LDH were found to be 99.5 mg g^{-1} and 80.3 mg g^{-1}, respectively. A one-pot in situ hydrothermal approach[137] was used to manufacture magnesium–aluminum double hydroxides (Mg–Al LDHs) to remove arsenate and phosphate oxo-anions from their aqueous solution. Maximum removal capacities for phosphate and arsenate from Mg–Al LDH produced with a 2:1 molar ratio of Mg and Al at 150 °C were found to be 33.2 mg g^{-1} and 56.3 mg g^{-1}, respectively. It was proposed that the ion exchange process occurred when nitrate interlayer anions swapped arsenate or phosphate anions. However, a coordination mechanism was proposed for mixed anionic solutions. Fe–Mg–Mn-LDH was prepared using the co-precipitation approach.[140] Ion exchange and electrostatic attraction were used to remediate the nitrate anions on the manufactured LDH adsorbent. Several mechanisms have been reported for the use of LDH in the remediation of environmental contaminants.

5.6.1 Physical adsorption. Because the layered double hydroxides have a relatively larger surface area and their surface contains both positively and negatively adsorptive active sites, physical adsorption occurs on their surface. Compared to the
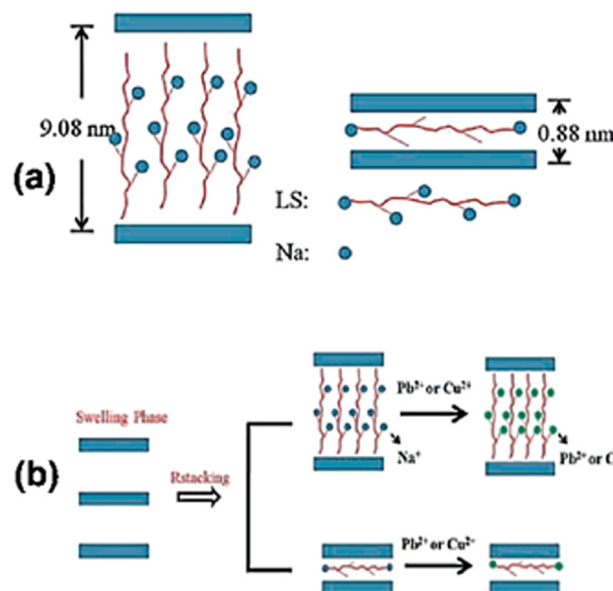

Fig. 12 Sketch presentation of (a) two existing ways of LS in the MgAl/(LDH) interlayer and (b) attachment of Cu^{2+} and Pb^{2+} with LS-LDH.

most well-known conventional adsorbents, they have enhanced adsorption capabilities. The adsorption capacity of the layered double hydroxides (LDH) can be modified by calcining their structures at high temperatures of up to 700 °C to produce their oxide forms.

5.6.2 Ion exchange mechanism. This occurs efficiently in the presence of charged pollutants and results in the swapping of the cations and anions existing in the medium for the structural anions or cations offered in the interlayer network of LDHs. This process may also be linked to the chelation of ionic species via the d-transition in the crystalline construction of LDHs.

The adsorption mechanism of the different toxic contaminants on LDH-containing hybrids mainly depends on the type of hybridizing material (adsorbent) and pollutant (adsorbate). Generally, physical adsorption, hydroxide precipitation, anion-metal complexes, electrostatic interaction, π–π interactions, and chemical bonding are common mechanisms involved in the adsorption process of LDH-containing hybrids.[141] In anionic/LDH, the adsorption of heavy metal ions is associated with the formation of anion-metal complexes and hydroxide precipitation on LDH surfaces through chemical bonding with the hydroxyl groups of LDH.[142]

Fig. 12a and b depicts the attachment of Cu^{2+} and Pb^{2+} through an ion-exchange mechanism on the sulfonated lignin (LS)/LDH.[143] Ma et al.[144] studied the adsorption of metal ions on intercalated LDH-containing polysulfide. After the formation of polysulfide–metal complexes, the LDH-containing polysulfide is converted into pristine LDH. The reaction schematic is presented in Fig. 12b.

6. Conclusion and future directions

Research has shown that the function of anion exchange for LDH may be efficiently regulated by substituting the layer-

forming cation. However, they simply pay attention to the phenotypic and morphological descriptions of their structures, and they employ the LDH findings without further investigating and evaluating the function of this mechanism. The function of metal cation coordination in binary or multi-component LDH systems, and the change of their crystalline structure, is to govern and regulate the corresponding crystallinity and crystal constructions. However, in the Ni–Fe system LDHs, only the coordination interaction among the metal cations has been completely and systematically investigated. The literature in this area is excessively fragmented, and although horizontal and longitudinal comparison experiments are helpful tactics, no consistent theory has been developed. This gap may be addressed by further studies. It was discovered that the LDH materials improved with active carbon have not yet undergone sufficient analysis during the photolysis of newly discovered contaminants and require additional in-depth experimental research in the future.

1. The biomass sources used to prepare the activated carbons that are mixed with LDHs must be varied. There are several biomass sources of carbon nowadays, but investigations suggest that only a few numbers of them can be used to commercially create LDH composites. Future investigations on the process of producing LDH from biomass carbon are needed.

2. The mechanistic study used to explain how LDH–carbon composites break down organic contaminants is not exact enough. It is now known that active radicals perform well in photocatalytic decomposition processes. However, it is still unknown how adding carbon elements to composites improves their ability to decompose pollutants and how this affects efficiency or transmission channels. Whether photo-generated electrons are not fully characterized is uncertain. Future studies will focus on the process by which LDH-C breaks down organic hazardous waste.

3. The investigation of additional factors for the industrialization of wastewater cleanup is emerging; research should be directed toward pilot plants and industrial manufacturing.

Data availability

No primary research results, software or code has been included and no new data were generated or analysed as part of this review.

Conflicts of interest

The authors declare that they have no conflict of interest.

Acknowledgements

References

1 P. Kuśtrowski, D. Sułkowska, L. Chmielarz and R. Dziembaj, *Appl. Catal., A*, 2006, **302**, 317–324.

2 L. Meili, P. V. Lins, C. L. P. S. Zanta, J. I. Soletti, L. M. O. Ribeiro, C. B. Dornelas, T. L. Silva and M. G. A. Vieira, *Appl. Clay Sci.*, 2019, **168**, 11–20.

3 P. Lins, D. Henrique, A. Ide, C. Zanta and L. Meili, *Sci. Pollut. Res.*, 2019, **26**, 31804–31811.

4 A. Navajas, I. Campo, A. Moral, J. Echave, O. Sanz, M. Montes and J. A. Odriozola, *Fuel*, 2018, **211**, 173–181.

5 M. Hájek, A. Tomášová, J. Kocík and V. Podzemna, *Appl. Clay Sci.*, 2018, **154**, 28–35.

6 A. Vaccari, *Appl. Clay Sci.*, 1999, **14**, 161–198.

7 G. Hincapié, D. López and A. Moreno, *Catal. Today*, 2018, **302**, 277–285.

8 H. Griffiths, *Layered Double Hydroxides: Structure, Synthesis and Catalytic Applications*, 2012.

9 V. Cunha, A. M. Da Costa Ferreira, V. Constantino, J. Tronto and J. Valim, *Quim. Nova*, 2009, **33**, 159–171.

10 J. Chen, C. Wang, Y. Zhang, Z. Guo, Y. Luo and C.-J. Mao, *Appl. Surf. Sci.*, 2019, **506**, 144999.

11 J. Gonçalves, P. Martins, L. Angnes and K. Araki, *New J. Chem.*, 2020, **44**, 9981–9997.

12 A. L. Johnston, E. Lester, O. Williams and R. L. Gomes, *J. Environ. Chem. Eng.*, 2021, **9**, 105197.

13 L. Wu, F.-S. Pan, Y. Liu, G. Zhang, A. Tang and A. Atrens, *Surf. Eng.*, 2017, **34**, 1–8.

14 M. A. Ahmed and A. A. Mohamed, *Inorg. Chem. Commun.*, 2023, **148**, 110325.

15 A. Iqbal and M. Fedel, *Coatings*, 2019, **9**, 30.

16 G. M. Tomboc, T. Kim, S. Jung, H. J. Yoon and K. Lee, *Small*, 2022, **18**, 1842–1855.

17 S. Nayak and K. Parida, *Catalysts*, 2021, **11**, 1072.

18 L. C. D. Agostino, R. G. L. Gonçalves, C. V. Santilli and S. H. Pulcinelli, *Sociedade Brasileira de Pesquisa de Materiais*, Brazil, 2019.

19 L. Valeikiene, M. Roshchina, I. Grigoraviciute-Puroniene, V. Prozorovich, A. Zarkov, A. Ivanets and A. Kareiva, *Crystals*, 2020, **10**, 470.

20 A. Farhan, A. Khalid, N. Maqsood, S. Iftekhar, H. M. A. Sharif, F. Qi, M. Sillanpaa and M. B. Asifi, *Sci. Total Environ.*, 2024, **912**, 169160.

21 L. Čapek, P. Kutálek, L. Smoláková, M. Hájek, I. Troppová and D. Kubička, *Top. Catal.*, 2013, **56**, 586–593.

22 R. Gabriel, S. Carvalho, J. Duarte, L. Oliveira, D. A. Giannakoudakis, K. Triantafyllidis, J. Soletti and L. Meili, *Appl. Catal., A*, 2021, **630**, 118470.

23 N. Balsamo, K. Sapag, M. Oliva, G. Pecchi, G. Eimer and M. Crivello, *Catal. Today*, 2016, **279**, 209–216.

24 R. Yang, Y. Gao, J. Wang and Q. Wang, Layered double hydroxide (LDH) derived catalysts for simultaneous catalytic removal of soot and NO_x, *Dalton Trans.*, 2014, **43**, 10317–10327.

25 C. Noda Pérez, C. A. Pérez, C. A. Henriques and J. L. F. Monteiro, *Appl. Catal., A*, 2004, **272**, 229–240.

26 M. Mostafa, M. Betiha, A. Rabie, H. Hassan and A. Morshedy, *Ind. Eng. Chem. Res.*, 2017, **57**(2), 425–433.

27 Y. M. Zheng, N. Li and W.-D. Zhang, *Colloids Surf., A*, 2012, **415**, 195–201.

28 R. Shabbir, A. Gu, J. Chen, M. Khan, P. Wang, Y. Jiao, Z. Zhang, Y. Liu and Y. Yang, *Int. J. Environ. Anal. Chem.*, 2020, **102**, 1–18.

29 H. Wang, Q. Fan, Z. Yang, S. Tang, C. Jingye and Y. Wu, *Mol. Catal.*, 2019, **468**, 1–8.

30 E. Musella, I. Gualandi, G. Ferrari, D. Mastroianni, E. Scavetta, M. Giorgetti, A. Migliori, M. Christian, V. Morandi, R. Denecke, M. Gazzano and D. Tonelli, *Electrochim. Acta*, 2021, **365**, 137294.

31 J. Li, L. Yan, Y. Yang, X. Zhang, R. Zhu and H. Yu, *New J. Chem.*, 2019, **43**, 15915–15923.

32 M. Sousa, F. Tourinho and J. Rubim, *J. Raman Spectrosc.*, 2000, **31**, 185–191.

33 T. Kloprogge, M. Weier, I. Crespo, M. Ulibarri, C. Barriga, V. Rives, W. Martens and R. L. Frost, *J. Solid State Chem.*, 2004, **177**, 1382–1387.

34 L. Miranda, C. Bellato, M. Fontes, M. Fabiano de Almeida, J. Milagres and L. Minim, *Chem. Eng. J.*, 2014, **254**, 88–97.

35 C. Hobbs, S. Jaskaniec, E. McCarthy, C. Downing, K. Opelt, K. Güth, A. Shmeliov, M. Mourad, K. Mandel and V. Nicolosi, *npj 2D Mater. Appl.*, 2018, **2**, 4–10.

36 F. Dionigi, Z. Zeng, I. Sinev, T. Merzdorf, S. Deshpande, M. B. Lopez, S. Kunze, I. Zegkinoglou, H. Sarodnik, D. Fan, A. Bergmann, J. Drnec, J. F. de Araujo, M. Gliech, D. Teschner, J. Zhu, W. X. Li, J. Greeley, B. R. Cuenya and P. Strasser, *Nat. Commun.*, 2020, **11**, 2522.

37 A. M. Rabie, E. A. Mohammed and N. A. Negm, *J. Mol. Liq.*, 2018, **254**, 260–266.

38 N. A. Negm, A. M. Rabie and E. A. Mohammed, Molecular interaction of heterogeneous catalyst in catalytic cracking process of vegetable oils: chromatographic and biofuel performance investigation, *Appl. Catal., B*, 2018, **239**, 36–45.

39 N. A. Negm, G. H. Sayed, F. Z. Yehia, O. I. Habib and E. A. Mohamed, *J. Mol. Liq.*, 2017, **234**, 157–163.

40 N. A. Negm, G. H. Sayed, O. I. Habib, F. Z. Yehia and E. A. Mohamed, *J. Mol. Liq.*, 2017, **237**, 38–45.

41 N. A. Negm, G. H. Sayed, F. Z. Yehia, O. I. H. Dimitry, A. M. Rabie and E. A. M. Azmy, *Egypt. J. Chem.*, 2016, **59**, 1045–1060.

42 H. A. Ahmed, A. A. Altalhi, S. A. Elbanna, H. A. El-Saied, A. A. Farag, N. A. Negm and E. A. Mohamed, *ACS Omega*, 2022, **7**, 4585–4594.

43 A. A. Altalhi, S. M. Morsy, M. T. H. Abou Kana, N. A. Negm and E. A. Mohamed, *Alexandria Eng. J.*, 2022, **61**, 4847–4861.

44 E. A. Mohamed, M. A. Betiha and N. A. Negm, *Energy Fuels*, 2023, **37**, 2631–2647.

45 S. Ha Lee, S. M. Tawfik, D. T. Thangadurai and Y.-I. Lee, *Microchem. J.*, 2021, **164**, 106010.

46 B. A. A. Balboul, A. A. Abdelrahman, H. M. Salem, E. A. Mohamed, D. I. Osman and A. M. Rabie, *J. Mol. Liq.*, 2022, **367**, 120562.

47 J. Shumaker, C. Crofcheck, S. Tackett, E. Santillan-Jimenez, T. Morgan, Y. Ji, M. Crocker and T. Toops, *Appl. Catal., B*, 2008, **82**, 101–120.

48 N. Bálsamo, S. Mendieta, A. Heredia and M. Crivello, *Mol. Catal.*, 2020, **481**, 110290.

49 D. G. Cantrell, L. J. Gillie, A. F. Lee and K. Wilson, *Appl. Catal., A*, 2005, **287**, 183–190.

50 P.-L. Boey, G. P. Maniam and S. Hamid, *Bioresour. Technol.*, 2009, **100**, 6362–6368.

51 S. Sankaranarayanan, C. A. Antonyraj and S. Kannan, *Bioresour. Technol.*, 2012, **109**, 57–62.

52 R. Prado, G. Almeida, M. Carvalho, L. Galvao, C. Cardoso Bejan, L. Costa, F. Pinto, J. Tronto and D. Pasa, *Catal. Lett.*, 2014, **144**, 1062–1073.

53 S. Yan, S. O. Salley and K. Y. Simon Ng, *Appl. Catal., A*, 2009, **353**, 203–212.

54 T. Montanari, M. Sisani, M. Nocchetti, R. Vivani, C. Herrera, G. Ramis, G. Busca and U. Costantino, *Catal. Today*, 2010, **152**, 104–109.

55 R. Gabriel, S. H. V. de Carvalho, J. L. S. Duarte, L. M. T. Oliveira, D. A. Giannakoudakis, K. S. Triantafyllidis, J. I. Soletti and L. Meili, *Appl. Catal., A*, 2022, **630**, 118470.

56 L. Fereidooni, A. Pirkarami, E. Ghasemi and A. Kasaeian, *Energy Convers. Manage.*, 2023, **296**, 117646.

57 G. Arzamendi, E. Arguiñarena, I. Campo, S. Zabala and L. M. Gandía, *Catal. Today*, 2008, **135**, 305–313.

58 D. Wang, X. Zhang, C. Liu, T. Cheng, W. Wei and Y. Sun, *Appl. Catal., A*, 2015, **505**, 478–486.

59 A. Stamate, O. D. Pavel and R. Zavoianu, *Catalysts*, 2020, **10**, 57.

60 C. Kajdas, *Lubr. Sci.*, 1994, **6**, 203–228.

61 Y. Wang, M. Zhang, Y. Liu, Z. Zheng, B. Liu, M. Chen, G. Guan and K. Yan, *Adv. Sci.*, 2023, **10**, 1–28.

62 K. Yan, Y. Liu, Y. Lu, J. Chai and L. Sun, *Catal. Sci. Technol.*, 2017, **7**, 1622–1645.

63 M. Zhang, Y. Liu, B. Liu, Z. Chen, H. Xu and K. Yan, *ACS Catal.*, 2020, **10**, 5179–5189.

64 J. Zhang, J. Sun and Y. Wang, *Green Chem.*, 2020, **22**, 1072–1098.

65 Y. Zeng, L. Lin, D. Hu, Z. Jiang, S. Saeed, R. Guo, I. Ashour and K. Yan, *Catal. Today*, 2023, **423**, 114252.

66 V. Rives, D. Carriazo and C. Martin, *Pillared clays and related catalysts*, 2010, 12, pp. 319–397.

67 X. Wang, C. Shang, G. Wu, X. Liu and H. Liu, *Catalysts*, 2016, **6**(1), 14.

68 J. C. Manayil, S. Sankaranarayanan, D. Bhadoria and K. Srinivasan, *Ind. Eng. Chem. Res.*, 2011, **50**, 13380–13386.

69 G. Wu, X. Wang, J. Li, N. Zhao and Y. Sun, *Catal. Today*, 2008, **131**, 402–407.

70 L. S. Randarevich, I. Z. Zhuravlev, V. V. Strelko, N. M. Patrilyak and T. A. Shaposhnikova, *J. Water Chem. Technol.*, 2009, **31**, 110–114.

71 A. Tsyganok, R. G. Green, J. B. Giorgi and A. Sayari, *Catal. Commun.*, 2007, **8**, 2186–2193.

72 F. Malherbe, C. Depège, C. Forano, J. P. Besse, M. P. Atkins, B. Sharma and S. R. Wade, *Appl. Clay Sci.*, 1998, **13**, 451–466.

73 A. L. Villa, D. E. De Vos, F. Verpoort, B. F. Sels and P. A. Jacobs, *J. Catal.*, 2001, **198**, 223–231.

74 A. Maciuca, E. Dumitriu, F. Fajula and V. Hulea, *Appl. Catal., A*, 2008, **338**, 1–8.

75 H. D. Smith, G. M. Parkinson and R. D. Hart, *J. Cryst. Growth*, 2005, **275**, 1665–1671.

76 S. Soled, D. Levin, S. Miseo and J. Ying, *Prep. Catal. VII*, Elsevier, 1998, pp. 359–367.

77 J. Zhao, J. Liu, Q. Han and L. Chen, *CrystEngComm*, 2016, **18**, 842–862.

78 M. Del Arco, D. Carriazo, S. Gutiérrez, C. Martín and V. Rives, *Inorg. Chem.*, 2004, **43**(1), 375–384.

79 B. M. Choudary, T. Someshwar, C. V. Reddy, M. L. Kantam, K. J. Ratnam and L. V. Sivaji, *Appl. Catal., A*, 2003, **251**, 397–409.

80 B. Sels, D. De Vos, M. Buntinx, F. Plerard, A. Kirsch-De Mesmaeker and P. Jacobs, *Nature*, 1999, **400**, 855–857.

81 J. Palomeque, F. Figueras and G. Gelbard, *Appl. Catal., A*, 2006, **300**, 100–108.

82 D. Carriazo, S. Lima, C. Martín, M. Pillinger, A. A. Valente and V. Rives, *J. Phys. Chem. Solids*, 2007, **68**, 1872–1880.

83 Y. Hanifah, R. Mohadi, M. Mardiyanto and A. Lesbani, *Ecol. Eng. Environ. Technol.*, 2023, **24**, 109–116.

84 B. Zeynizadeh and M. Gilanizadeh, *New J. Chem.*, 2019, **43**, 18794–18804.

85 E. Stamate, O. D. Pavel, R. Zăvoianu, B. Ioana, A. Ciorîta, R. Birjega, K. Neubauer, A. Köckritz and I. C. Marcu, *Materials*, 2021, **14**, 7457.

86 N. Ahmed, R. Menzel, Y. Wang, A. García, S. Bawaked, A. Obaid, S. Basahel and M. Mostafa, *J. Solid State Chem.*, 2016, **246**, 130–137.

87 M. García Álvarez, D. Crivoi, F. Medina and D. Tichit, *ChemEngineering*, 2019, **3**(1), 29.

88 N. Ma, Y. Song, F. Han, G. Waterhouse, Y. Li and S. Ai, *Catal. Sci. Technol.*, 2020, **10**, 4010–4018.

89 S. Xia, L. Zheng, W. Ning, L. Wang, P. Chen and Z. Hou, *J. Mater. Chem. A*, 2013, **1**, 11548–11552.

90 Y. Yang, W. Zhu, D. Cui and C. Lü, *Appl. Clay Sci.*, 2021, **200**, 105958.

91 D. Tichit, G. Layrac and C. Gerardin, *Chem. Eng. J.*, 2019, **369**, 302–332.

92 Z. Georgiopoulou, A. Verykios, K. Ladomenou, K. Maskanaki, G. Chatzigiannakis, K.-K. Armadorou, L. Palilis, A. Chroneos, S. Gardelis, A. Yusoff, T. Coutsolelos, K. Aidinis, M. Vasilopoulou and A. Soultati, *Nanomaterials*, 2022, **13**, 169.

93 G. Fan, D. Evans and X. Duan, *Chem. Soc. Rev.*, 2014, **43**, 7040–7066.

94 X. Wu, Y. Du, X. An and X. Xie, *Catal. Commun.*, 2014, **50**, 44–48.

95 Z. Wang, C. Li and K. Domen, *Chem. Soc. Rev.*, 2019, **48**, 2109–2125.

96 J. S. Schubert, J. Popovic, G. M. Haselmann, S. P. Nandan, J. Wang, A. Giesriegl, A. S. Cherevan and D. Eder, *J. Mater. Chem. A*, 2019, **7**, 18568–18579.

97 S. F. Ng, M. Y. L. Lau and W. J. Ong, *Sol. RRL*, 2021, 2000535.

98 Y. Zhao, G. I. N. Waterhouse, G. Chen, X. Xiong, L.-Z. Wu, C.-H. Tung and T. Zhang, *Chem. Soc. Rev.*, 2019, **48**, 1972–2010.

99 H. Boumeriame, E. S. Da Silva, A. S. Cherevan, T. Chafik, J. L. Faria and D. Eder, *J. Energy Chem.*, 2022, **64**, 406–431.

100 Y. Wang, Y. Zhang, Z. Liu, C. Xie, S. Feng, D. Liu, M. Shao and S. Wang, *Angew. Chem., Int. Ed.*, 2017, **56**, 5867.

101 S. Dou, L. Tao, R. Wang, S. E. Hankari, R. Chen and S. Wang, *Adv. Mater.*, 2018, **30**, 1705850.

102 Y. Zhao, G. Waterhouse, G. Chen, X. Xiong, L.-Z. Wu, C.-H. Tung and T. Zhang, *Chem. Soc. Rev.*, 2019, **48**, 1972–2010.

103 X. Sun, L. Shi, H. Huang, X. Song and T. Ma, *Chem. Commun.*, 2020, **56**, 11000–11013.

104 X. Lu, H. Xue, H. Gong, M. Bai, D.-M. Tang, R. Ma and T. Sasaki, *Nano-Micro Lett.*, 2020, **12**, 86.

105 D. Tang, J. Liu, X. Wu, R. Liu, X. Han, Y. Han, H. Huang, Y. Liu and Z. H. Kang, *ACS Appl. Mater. Interfaces*, 2014, **6**(10), 7918–7925.

106 W. Ma, R. Ma, C. Wang, J. Liang, X. Liu, K. Zhou and T. Sasaki, *ACS Nano*, 2015, **9**(2), 1977–1984.

107 G. Shi, C. Yu, Z. Fan, J. Li and M. Yuan, *ACS Appl. Mater. Interfaces*, 2018, **11**(3), 2662–2669.

108 T. Bhowmik, M. Kundu and S. Barman, *ACS Appl. Energy Mater.*, 2018, **1**(3), 1200–1209.

109 L. Yipu, X. Liang, L. Gu, Y. Zhang, G.-D. Li, X. Zou and J. Chen, *Nat. Commun.*, 2018, **9**, 2609.

110 Z. Yan, H. Sun, X. Chen, H. Liu, Y. Zhao, H. Li, W. Xie, F. Cheng and J. Chen, *Nat. Commun.*, 2018, **9**, 2373.

111 X. Lu and C. Zhao, *Nat. Commun.*, 2015, **6**, 6616.

112 Q. Wang, X.-X. Xue, Y. Lei, Y. Wang, Y. Feng, X. Xiong, D. Wang and Y. Li, *Small*, 2020, **16**, 2001571.

113 T. Ling, T. Zhang, B. Ge, L. Han, L. Zheng, F. Lin, Z. Xu, W. Hu, X. Du, K. Davey and S. Qiao, *Adv. Mater.*, 2019, **31**, 1807771.

114 F. Guozhao, W. Qichen, J. Zhou, Z. Chen, Z. Wang, A. Pan and S. Liang, *ACS Nano*, 2019, **13**(5), 5635–5645.

115 J. F. Qin, M. Yang, T. S. Chen, B. Dong, S. Hou, X. Ma, Y. N. Zhou, X. L. Yang, J. Nan and Y. M. Chai, *Int. J. Hydrogen Energy*, 2019, **45**, 2745–2753.

116 C. Lei, W. Zhou, Q. Feng, Y. Zhang, Y. Chen and J. Qin, *Nano-Micro Lett.*, 2019, **11**, 45.

117 R. Li, J. Wang, B. Zhou, M. K. Awasthi, A. Ali, Z. Zhang, L. Gaston, A. Lahori, D. A. Mahar and J. Gan, *Sci. Total Environ.*, 2016, **559**, 121–129.

118 Y. Yang, W. Zhang, Y. Xiao, Z. Shi, X. Cao, Y. Tang and Q. Gao, *Appl. Catal., B*, 2018, **242**, 132–139.

119 H. Liang, A. N. Gandi, C. Xia, M. N. Hedhili, D. H. Anjum, U. Schwingenschlögl and H. N. Alshareef, *ACS Energy Lett.*, 2017, **2**, 1035–1042.

120 K. He, T. Tsega, X. Liu, J. Zai, X.-H. Li, X. Liu, W. Li, N. Ali and X. Qian, *Angew. Chem., Int. Ed.*, 2019, **58**, 11903–11909.

121 H. Zhang, X. Li, A. Hähnel, V. Naumann, C. Lin, S. Azimi, S. Schweizer, W. Maijenburg and R. Wehrspohn, *Adv. Funct. Mater.*, 2018, **28**, 1706847.

122 M. N. Nimbalkar and B. R. Bhat, *J. Environ. Chem. Eng.*, 2021, **9**, 106216.

123 A. Yadav, N. Bagotia, A. Sharma and S. Kumar, *Sci. Total Environ.*, 2021, **784**, 147108.

124 A. Yadav, N. Bagotia, A. Sharma and S. Kumar, *Sci. Total Environ.*, 2021, **799**, 149500.

125 D. Ahmed, L. Naji, A. Faisal, N. Al-Ansari and M. Naushad, *Sci. Rep.*, 2020, **10**, 2042.

126 A. Farhan, J. Arshad, E. U. Rashid, H. Ahmad, S. Nawaz, J. Munawar, J. Zdarta, T. Jesionowski and M. Bilal, *Chemosphere*, 2023, **310**, 136835.

127 M. El-Abboubi, N. Taoufik, F. Kzaiber, N. Barka, F. Z. Mahjoubi and O. Abdelkhalek, Sorption of methyl orange dye by dodecyl-sulfate intercalated Mg–Al layered double hydroxides, *Mater. Today Proc.*, 2020, **37**, 3894–3897.

128 M. Kostić, S. Najdanović, N. Velinov, M. Radović Vučić, M. Petrović, J. Mitrović and A. Bojić, *Environ. Technol. Innovation*, 2022, **26**, 102358.

129 M. Mureseanu, A. Eliescu, E. C. Ignat, G. Carja and N. Cioatera, *C. R. Chim.*, 2022, **25**, 1–12.

130 R. Gayathri, G. Kannappan Panchamoorthy and P. Kumar, *Chemosphere*, 2020, **262**, 128031.

131 A. Amer, G. H. Sayed, R. M. Ramadan, A. M. Rabie, N. A. Negm, A. A. Farag and E. A. Mohamed, *J. Mol. Liq.*, 2021, **341**, 116935.

132 M. R. Pérez, I. Pavlovic, C. Barriga, J. Cornejo, M. C. Hermosín and M. A. Ulibarri, *Appl. Clay Sci.*, 2006, **32**, 245–251.

133 X. Zhang, R. Shan, X. Li, L. Yan, Z. Ma, R. Jia and S. Sun, *Water Sci. Technol.*, 2021, **83**(4), 975–984.

134 M. Dinari and S. Neamati, *Colloids Surf., A*, 2020, **589**, 124438.

135 L. Guo, Y. Zhang, J. Zheng, L. Shang, Y. Shi, Q. Wu, X. Liu, Y. Wang, L. Shi and Q. Shao, *Adv. Compos. Hybrid Mater.*, 2021, **4**, 1–11.

136 S. Somma, E. Reverchon and L. Baldino, *ChemEngineering*, 2021, **5**, 47.

137 K. W. Jung, S. Y. Lee, J. W. Choi, M. J. Hwang and W. G. Shim, *Chem. Eng. J.*, 2021, **420**, 129775.

138 S. Li, X. Ma, Z. Ma, X. Dong, Z. Wei, X. Liu and L. Zhu, *Environ. Technol. Innovation*, 2021, **23**, 101771.

139 M. Motandi, Z. Zhang, I. Stelgen and L. Yan, *Environ. Prog. Sustainable Energy*, 2021, **41**, 13744.

140 H. Zhou, Y. Tan, W. Gao, Y. Zhang and Y. Yang, *Sci. Rep.*, 2020, **10**, 16126.

141 L. Tan, Y. Wang, Q. Liu, J. Wang, X. Jing, L. Liu, J. Liu and D. Song, *Chem. Eng. J.*, 2015, **259**, 752–760.

142 N. Wang, J. Sun, H. Fan and S. Ai, *Talanta*, 2016, **148**, 301–307.

143 G. Huang, D. Wang, S. Ma, J. Chen, L. Jiang and P. Wang, *J. Colloid Interface Sci.*, 2015, **445**, 294–302.

144 S. Ma, Q. Chen, H. Li, P. Wang, S. M. Islam, Q. Gu, X. Yang and M. G. Kanatzidis, *J. Mater. Chem. A*, 2014, **2**, 10280–10289.